PCCP

Tuning the Work Function of Nickel Oxide using Triethoxysilane Functionalized Monolayers

Journal:	*Physical Chemistry Chemical Physics*
Manuscript ID	CP-ART-06-2020-003306.R3
Article Type:	Paper
Date Submitted by the Author:	16-Dec-2020

Complete List of Authors:	Chen, Gang; Colorado School of Mines, Department of Physics Wang, Xinquan; Colorado School of Mines, Department of Physics Shi, Yuting; Colorado School of Mines, Department of Chemistry Tinkham, Jonathan; Colorado School of Mines, Department of Chemistry Brenner, Thomas; Colorado School of Mines, Department of Physics; Weizmann Institute of Science, Department of Materials and Interfaces Olson, Dana; National Renewable Energy Laboratory; DNV GL Furtak, Thomas; Colorado School of Mines, Department of Physics Sellinger, Alan; Colorado School of Mines, Department of Chemistry

PCCP

ARTICLE TYPE

Cite this: DOI: 00.0000/xxxxxxxxxx

Tuning the Work Function of Nickel Oxide using Triethoxysilane Functionalized Monolayers

Gang Chen,[a] Xinquan Wang,[a] Yuting Shi,[b] Jonathan S. Tinkham,[b] Thomas M. Brenner,[a‡] Dana C. Olson,[c§] Alan Sellinger,[b*] and Thomas E. Furtak[a*]

Received Date
Accepted Date

DOI: 00.0000/xxxxxxxxxx

The work function of nickel oxide (NiO_x) electrodes was tuned by the covalent attachment of commercially available as well as specially synthesized triethoxysilane functionalized molecules with a range of dipole moments. The presence of the silane molecular layers on the NiO_x surface was verified using Fourier transform infrared (FTIR) spectroscopy and contact angle measurements. While these tests indicated the surface coverage was incomplete, Kelvin probe measurements showed that the coverage was sufficient to change the work function of the NiO_x across a range of ∼900 meV. Density functional theory (DFT) calculations of the dipole moments of the isolated molecules correlated well with the measured work function changes.

1 Introduction

Organic bulk heterojunction (BHJ) photovoltaic devices, and more recently, organic perovskite solar cells, hold the promise of low cost solution processing with relatively high energy conversion efficiencies[1–6]. The carrier collecting contacts of these devices typically involve layers with hole and/or electron charge selective properties in order to minimize the charge recombination at the electrodes and increase the energy conversion efficiency[2,4,7–9]. Many BHJ device structures incorporate a layer of poly(3,4-ethylenedioxythiophene):poly(styrenesulfonate) (PEDOT:PSS) as the hole transport and electron-blocking layer. Unfortunately, the presence of this layer has been linked to device degradation under air exposure as it absorbs water from the ambient environment[10,11]. Also the acidic nature of PEDOT:PSS limits its use with pH sensitive transparent conducting oxides such as indium tin oxide (ITO)[12,13].

Recent years have witnessed the successful application of different metal oxides, such as MoO_3[14–16], V_2O_5[14,17–19], WO_3[14,20–23] and NiO_x[7,24–28], as alternative hole transport layers (HTL) in organic photovoltaic (OPV) and perovskite devices. Particularly, solution processed NiO_x has been shown to outperform PEDOT:PSS in BHJ devices and to improve device stability[25,29]. The usefulness of NiO_x as an HTL arises from: (i) an alignment of the NiO_x valence band with the highest occupied molecular orbital (HOMO) of several BHJ donor materials; (ii) a large band gap that places the conduction band closer to the vacuum level than the lowest unoccupied molecular orbital (LUMO) of typical fullerene acceptors in BHJ devices (thus blocking electron transport); (iii) higher hole mobility relative to the electron mobility, (iv) the potential for improved interfacial morphology and (v) good optical transparency.

Apart from OPV devices, NiO_x has been successfully utilized as an HTL in perovskite solar cells[30,31] and heterojunction crystalline silicon solar cells[32]. For many of these device structures, control of the oxygen defect structure through O_2 plasma treatments, UV ozone treatments, or deposition conditions (e.g. oxygen partial pressure during sputtering) was required to improve device performance. This was often attributed to an increase in the work function of the NiO_x and better alignment of its valence band with BHJ HOMO levels[24–27,33,34]. The NiO_x work function change following these treatments was also reported to relax over time in an inert atmosphere[24]. However, air-exposed NiO_x is hydroxylated, which emparts sufficient stability to enable reproducible handling under ambient conditions[29,35].

In addition to its role as an HTL in photovoltaics, the work function of NiO_x is relevant in other applications where interfacial charge transfer is important. Solution processed NiO_x has been employed as a charge-injection layer in organic light-emitting diodes (OLEDs)[36], and as the channel layer in solution-processed thin film transistors (TFTs)[37]. Nickel oxide has also been demonstrated as an efficient (22% incident photon to current) photocathode in photoelectrochemical water splitting[38]. An understanding of the work function of nickel oxide and its sensitivity to adsorption is also fundamental to its use in gas sensing[39]. In these and other applications of NiO_x it is important to engineer

[a] Department of Physics, Colorado School of Mines, Golden, CO, USA.
[b] Department of Chemistry, Colorado School of Mines, Golden, CO, USA.
[c] National Renewable Energy Laboratory, Golden, CO, USA.
‡ Present address: Department of Materials and Interfaces, Weizmann Institute of Science, Rehovot, Israel.
§ Present address: DNV GL Energy, San Diego, CA, USA.
* Corresponding authors. Email: aselli@mines.edu; tfurtak@mines.edu.

the work function of the material.

Molecular dipolar surface modifiers provide an effective approach to altering the work function of metal oxides and optimizing interfacial energy level alignment, without changing the bulk properties of the bulk metal oxide. Dipolar molecular layer modification of ZnO[40–47] and ITO[48–58] have been studied extensively. By comparison, fewer studies have been reported on surface modification of NiO_x. Wang *et al.* demonstrated work functions changes of ∼100 meV on NiO_x nanoparticle films functionalized with benzoic acid derivatives having different dipole moments[59]. Cheng *et al.* argued that n-butylamine treatment of NiO_x can reduce the surface dipole moment of the material[60]. A few reports of NiO_x surface treatment with phosphonic or benzoic acids have also been published[61–63]. However, systematic modification of the NiO_x work function using molecules with different dipole moments were not explored. In addition, most of these approaches have involved surface modifiers that are acids, which can etch metal oxides[64].

In this study, a series of organic molecules with triethoxysilane (TES) attachment groups and different functional end groups were utilized to form molecular monolayers and modify the NiO_x surface. We used simple TES molecules that are commercially available, as well as specially synthesized TES materials that involved a carbon-carbon double bond (within a styryl group) in the link between the TES group and the dipole-adjusting group. The attachment chemistry in the present study followed an approach previously demonstrated on ZnO surfaces[65]. The modified NiO_x samples were characterized by contact angle measurement and Fourier Transform Infrared Spectroscopy (FTIR). Furthermore, the work functions of the unmodified and modified nickel oxide surfaces, determined using a Kelvin probe, were correlated with the dipole moment of the isolated TES molecules obtained from density functional theory (DFT) calculations. The work function control of NiO_x that we have demonstrated here will be important for organic device development in particular, since better energy level alignment at the NiO_x/organic interface reduces energy loss during hole extraction/injection and improves device performance[36,42,43,66].

2 Methods

Some of the surface modifiers used in this study were commercially available (Gelest, PA): triethoxy(octadecyl)silane (OTES), triethoxy(phenyl)silane (PTES), and (4-chlorophenyl)triethoxysilane (4CPTES). They are shown in Fig. 1. The materials with a double-bonded link that were synthesized for this study are shown in Fig. 2. The synthesis procedures are described below.

2.1 Specially synthesized materials

Solvents were purchased from Fisher (ACS grade) and Sigma-Aldrich and used as received. Palladium catalysts were purchased from Strem, Inc. All other chemicals were acquired from Sigma-Aldrich and used as received unless otherwise noted.

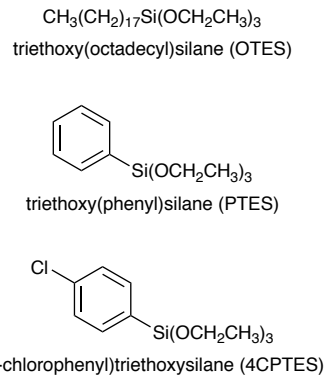

Fig. 1 Chemical structure of commercially available silanes, designated as OTES, PTES, and 4CPTES

2.1.1 (E)-triethoxy(4-methylstyryl)silane (ToTES)

In a glovebox, 4-bromotoluene (1.44 mL, 2.0 g, 11.6 mmol), $Pd[P(t\text{-}Bu)_3]_2$ (40 mg, 0.078 mmol), vinyl(triethyloxy)silane (2.5 mL, 2.3 g, 12 mmol), dicyclohexylmethylamine (2.5 mL, 2.28 g, 11.7 mmol, 0.7 mol %), and 20 mL toluene were added to a clean and dry schlenk flask. The flask was removed from the glovebox and attached to a schlenk line using argon gas.Using the Heidolph Heat-On® accessory, the reaction mixture was stirred at 85 C overnight, at which point an aliquot was taken for Thin Layer Chromatography (TLC) to determine reaction progress. Upon reaction completion the flask was cooled to room temperature and filtered to remove the dicyclohexylmethylamine hydrobromide salt. The filtrate was extracted with ethyl acetate and cold 5% HCl and then twice with DI water. The organic layer was dried over anhydrous $MgSO_4$ filtered and washed with additional ethyl acetate. The solvent was removed via rotavap to obtain the crude product as an orange oil. The crude product was purified by column chromatography (hexane:ethyl acetate) to provide a colorless oil. Yield 2.24 g, 69%.

^{1}H NMR (500 MHz, chloroform-*d*) δ= 7.39 (d, J = 8.0 Hz, 2H), 7.22 (d, J = 19.3 Hz, 1H), 7.15 (d, J = 7.9 Hz, 2H), 6.14 (d, J = 19.3 Hz, 1H), 3.91 (q, J = 7.0 Hz, 6H), 2.35 (s, 3H), 1.29 (t, J = 7.1 Hz, 9H).

^{13}C NMR (126 MHz, chloroform-*D*) δ=149.18, 138.82, 135.08, 129.35, 126.83, 116.38, 77.50, 77.25, 76.99, 58.65, 21.33, 18.38.

2.1.2 (E)-triethoxy(4-(trifluoromethyl)styryl)silane (CF3TES)

Following the procedure described above, with the 4-bromotoluene replaced by 2 g of 4-bromobenzotrifluoride, a colorless oil was obtained. Yield: 71%.

^{1}H NMR (500 MHz, chloroform-*d*) δ= 7.41 (d, J = 8.6 Hz, 2H), 7.16 (d, J = 19.3 Hz, 1H), 6.85 (d, J = 8.6 Hz, 2H), 6.00 (d, J = 19.3 Hz, 1H), 3.88 (q, J = 7.0 Hz, 6H), 3.78 (s, 3H), 1.26 (t, J = 7.0 Hz, 9H).

^{13}C NMR (126 MHz, chloroform-*d*) δ=160.25, 148.72, 130.66, 128.22, 114.73, 113.98, 58.63, 55.34, 18.36.

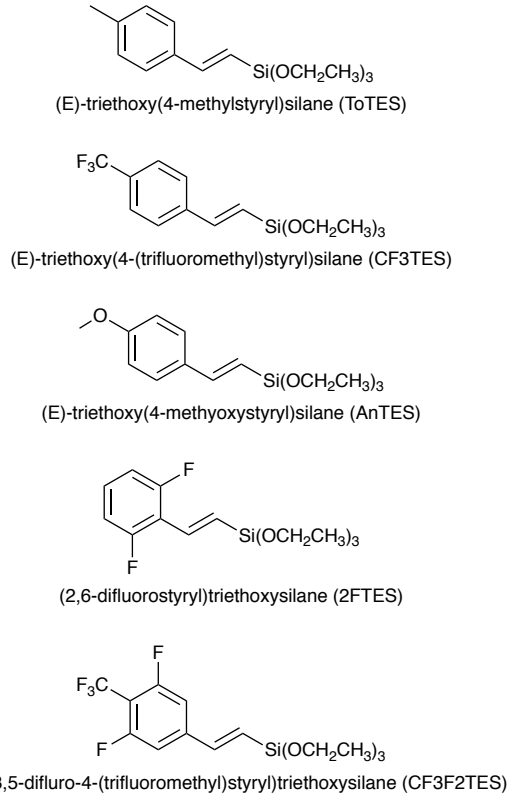

Fig. 2 Chemical structure of silanes synthesized for this study as described in Section 2.1.

2.1.3 (E)-triethoxy(4-methyoxylstyryl)silane (AnTES)

Following the procedure described above, with the 4-bromotoluene replaced by 2 g of 4-bromoanisole, an off-white oil was obtained. Yield: 35%.

^{1}H NMR (500 MHz, chloroform-*d*) δ= 7.41 (d, J = 8.6 Hz, 2H), 7.16 (d, J = 19.3 Hz, 1H), 6.85 (d, J = 8.6 Hz, 2H), 6.00 (d, J = 19.3 Hz, 1H), 3.88 (q, J = 7.0 Hz, 6H), 3.78 (s, 3H), 1.26 (t, J = 7.0 Hz, 9H).

^{13}C NMR (126 MHz, chloroform-*d*) δ=160.25, 148.72, 130.66, 128.22, 114.73, 113.98, 58.63, 55.34, 18.36.

2.1.4 (2,6-difluorostyryl)triethoxysilane (2FTES)

Following the procedure described above, with the 4-bromotoluene replaced by 2 g of 2-6-difluorobromobenzene, a colorless oil was obtained. Yield: 73%.

^{1}H NMR (500 MHz, DMSO-d_6) δ= 7.37 (m, 1H), 7.10 (t, 2H), 7.05 (d, 1H), 6.32 (d, 1H), 3.77 (m, 6.4H), 1.14 (t, 9H)

2.1.5 (E)-(3,5-difluoro-4-(trifluoromethyl)styryl)triethoxysilane (CF3F2TES)

Following the procedure described above, with the 4-bromotoluene replaced by 2 g of 3,5-difluoro-4-(trifluoromethyl)bromobenzene, a colorless oil was obtained. Yield: 73%.

^{1}H NMR (500 MHz, DMSO-d_6) δ= 7.65 (d, 2H), 7.10 (d, 1H), 6.61 (d, 1H), 3.78 (q, 6.7H), 1.15 (t, 9H).

2.2 Preparation of nickel oxide

ITO-coated glass or silicon substrates were cut into 1×1 inch squares. The substrates were cleaned by ultra-sonication in acetone and then in isopropyl alcohol for 15 min each, followed by ultraviolet-ozone (UVO) cleaning for at least 30 min. The synthesis of NiO_x films followed the method of Refs. 24,26, and 67. The deposition solution was prepared by adding 150 mg of nickel formate dihydrate (Sigma-Aldrich) to 3 ml of ethylene glycol (Sigma-Aldrich). Then, 150-200 microliters of ethylenediamine (Sigma-Aldrich) was added to help the nickel formate to dissolve. This solution was heated overnight at 50 C with a magnetic stir bar set to 400 rpm. It was sometimes necessary to add additional ethylenediamine and/or to increase the temperature to completely remove visible traces of solid nickel formate. The resulting solution, which was deep purple in color with the nickel in a complex as $[Ni(H_2N(CH_2)_2NH_2)_2](HCO_2)_2$, was purified by filtering it through a 0.45 micrometer nylon filter to remove any remaining undissolved material. The films were created on the substrates by spin-coating a small amount of this solution at 4000 rpm for 120 s. They were then annealed in air on a hotplate at 300 C for 60 min. The hotplate was then turned off and the film allowed to cool for 30 min before handling. This method leads to films that are generally $\sim$10 nm thick[24,26].

2.3 Triethoxysilane treatment

Attachment of TES-based molecules to NiO_x followed a method originally developed for attachment to SiO_2[68] and ZnO[65] surfaces. The procedure involves an amine-catalyzed condensation reaction between the triethoxysilane species and surface hydroxyls. This results in a covalently-bonded, surface-attached siloxane network with non-attached byproduct ethanols. Previous studies have shown that air-exposed nickel oxide has hydroxyl groups on the surface[29,35], making it a good candidate for this method.

The NiO_x samples were first baked in a 400 C oven for 20 min to remove physisorbed water. Thermal treatment to remove moisture from metal oxide surfaces is well documented in the literature[69,70]. It is typically necessary to use temperatures as high as 400 C to remove all forms of adsorbed water, while heating to the range of 600 C can remove hydroxyl species as well. In the case of NiO_x we know that the surface of the as-prepared material is covered with a combination of NiO, $Ni(OH)_2$, NiOOH, and H_2O[7]. While heating at 400 C removes the water, it also leads to a reproducible surface that, under ambient conditions, is quickly covered with surface OH[71]. It is these hydroxyl species that enable the TES attachment mechanism.

After the baking step the samples were allowed to cool in air for several minutes, and then placed in a solution of TES molecules at 45 C for 90 min. The TES solution consisted of 0.072 M n-butylamine and 0.045 M OTES or 0.09 M PTES/4CPTES in toluene. Liquid OTES, PTES and 4CPTES were used as received without further purification. Because the specially synthesized styryl-based TES molecules were available in only small amounts the concentration of these materials was reduced to $\sim$10% of the amounts cited above, while keeping the concentration of the other two components unchanged. Tests using commercially

available OTES showed this reduction in concentration did not have a significant effect on surface coverage. After the 90 min deposition treatment the samples were rinsed with toluene and acetone and blown dry with nitrogen. This was followed by heating in a 110 C oven for 60 min. Finally, the samples were rinsed again with toluene and acetone and blown dry with nitrogen.

As discussed in Walba et al.[68], atmospheric water appears to be necessary for successful attachment. We have hypothesized that ethoxy groups hydrolyze prior to the molecule's interaction with the surface. A reproducible level of water in the ambient above the toluene solution was provided by a water bath surrounding the toluene beaker, which was also employed to ensure a constant temperature during the deposition.

While surface modification with trichlorosilanes, which hydrolyze very rapidly leading to preoligomerization, are notoriously difficult to control[72] this is not the case with triethoxysilanes, which are much less reactive. The n-butylamine is a very important component of the process, since it acts as a catalyst with the ethoxysilanes to promote the condensation reaction at the surface. The details of the proposed mechanism are extensively discussed in Walba et al.[68]. In that study we have shown that the amine-catalyzed ethoxysilane process leads to covalently attached layers that are no more than one molecule thick, with no surface-attached oligomers.

2.4 Characterization

Normal incidence Fourier Transform Infrared (FTIR) transmission spectra were obtained using a Nicolet Magna-IR 560 equipped with a CaF beam splitter and a liquid-nitrogen-cooled mercury-cadmium-telluride detector. Each spectrum represents the average of 800 scans collected at 6 cm^{-1} resolution. The absorbance spectra were calculated as the negative of the base-10 logarithm of the transmission of the modified sample divided by the transmission of an unmodified NiO_x sample.

Contact angle measurements (CA) were performed using sessile drops of deionized water. A drop volume of approximately 2 μL was back-illuminated and photographed with a digital camera. The contour of the drop outline in the image was fit with a piecewise polynomial function whose slope at the two interface points of the silhouette determined the CA[73].

Differences in work function caused by different surface treatments were determined by contact potential difference (CPD) measurement in air using a KP Technology SKP5050 Kelvin Probe. The CPD of each treatment was measured with respect to a gold surface that had been exposed to the atmosphere for a long time. While the absolute work function of this surface was not known, it still provided a stable reference. The relative work function change of the modified NiO_x sample, $\Delta\phi$, was defined in reference to the unmodified NiO_x control surface, which was assigned a value of $\Delta\phi = 0$ meV.

Atomic force microscopy (AFM) was used to characterize the NiO_x surface topography. Imaging of the sample was carried out in tapping mode (Veeco, Nanoscope III) with high aspect ratio cantilever tips (Nanoworld, Switzerland). These tips had a radius of curvature of 2-5 nm with a half-cone angle <10° for the last 20 nm of the tip. The AFM tests were performed to verify that our films were structurally similar to those produced in Refs. 24,26, and 67. Additional structural, optical, and electronic properties of the NiO_x material in these films have been reported in those publications.

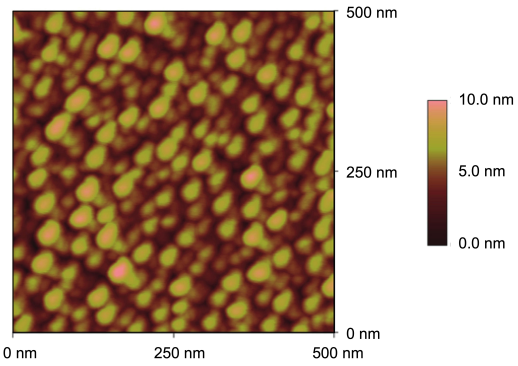

Fig. 3 AFM height image of control NiO_x on a silicon wafer. RMS roughness = 1.27 nm

2.5 Density Functional Theory (DFT) modeling of dipole moments

While it would be ideal to theoretically model the entire system consisting of the head group of the attached molecule and the surface bond involving the siloxane network attached to the nickel oxide, useful insight can be acquired through calculation of the molecular dipole of the gas phase species. This approach follows earlier work of ours[55] as well as others[49,50,74] where useful trends were identified. Accordingly, the Vienna Ab Initio Simulation Package (VASP) with B3LYP functional was utilized to calculate the dipole moment of isolated TES molecules. All structures were optimized with the energy cutoff of 800 eV within the 40 nm × 40 nm × 40 nm supercell, exploiting chemical constraints and local-atomic site symmetry, where possible. The results are expressed as the component of the dipole moment along the body axis of the molecule (through the 4 and 4' carbon atoms on the ring). The sign of the dipole reported here follows the physics convention (a vector directed from negative charge toward positive charge).

3 Results and Discussion

Figure 3 presents an AFM topographic image of a typical as-prepared film which was used as a control in the CPD measurements. Lateral structures (particles or grains) with an average size of ∼20 nm are observed. The dense NiO_x film has a RMS roughness of 1.27 nm, similar to what has been previously reported (∼1.35 nm) in a study of NiO_x prepared in the same way. As part of that study conductive tip AFM showed good conductivity at all lateral positions across the film.[26] AFM images recorded from NiO_x coated with TES materials were very similar to those obtained prior to coating, with no significant increase in the rms roughness beyond sample-to-sample variations. In one set of experiments the uncoated surface had an rms roughness of 1.66 nm.

After attachment of PTES this changed to 1.23 nm, while with OTES the rms roughness was smaller, 0.55 nm. A reduction of the roughness with OTES is not unexpected due to the long alkyl chain ($\tilde{2}$ nm for an all-trans conformation) in OTES, which could relax to fill the boundaries between grains.

The attachment chemistry was optimized using the three commercially available TES molecules and was then applied to the specially synthesized molecules, as well, because the latter were available in limited quantities. Figure 4 shows FTIR absorbance spectra of OTES-treated NiO_x surfaces in the spectral region of the C-H stretching modes. The presence of the symmetric and asymmetric methylene stretch peaks at 2852 cm^{-1} and 2924 cm^{-1}, respectively, which are associated with the OTES alkyl chains, confirms the presence of the molecule on the NiO_x surface. Also shown is the spectrum from a mechanically assembled Langmuir-Blodgett (LB) single monolayer of stearic acid, which has a similar length alkyl chain (C17, compared to C18 for OTES). The integrated intensity of the absorbance of the C-H stretch modes for the OTES layers is about 70% of that observed for the stearic acid layer, which suggests incomplete surface coverage. Our experience is that the OTES intensity is nearly the same for various samples and with different concentrations of OTES in the deposition solution, indicating that the coverage is self-limiting and stable. Consequently, we have assumed that a similar coverage is reached for each type of molecule, since their attachments involve the same surface reaction. The frequencies of the symmetric and asymmetric stretch modes of alkyl chains are known to be an indicator of the degree of order in the chains[75,76]. The values observed here are between those of the LB monolayer, representative of dense close-packed chains, and values reported for liquid-like chains at 2856 cm^{-1} and 2928 cm^{-1} [77]. This indicates that the TES monolayers on NiO_x are disordered. Also, n-butylamine was added to the deposition solution to act as a catalyst for the attachment chemistry[65,68]. A comparison of the infrared absorption spectra with and without n-butylamine in Fig. 4 makes it clear that including this catalyst in the deposition solution promotes the attachment of OTES to NiO_x. This is a strong indicator that the reaction mechanism involves conversion of surface hydroxyl groups and the triethoxysilyl species on the TES molecules into a covalently bonded Ni-O-Si surface-attached monolayer, as occurs on SiO_2 and ZnO.

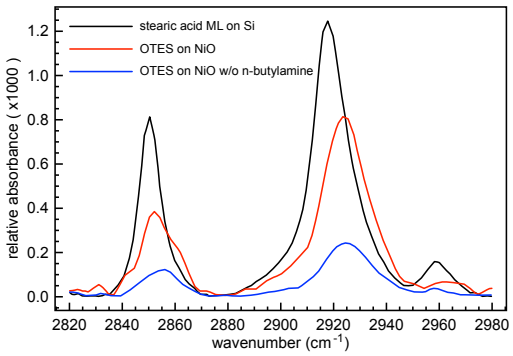

Fig. 4 Infrared absorbance in the C-H stretch region of OTES on NiO_x with (red) or without (blue) n-butylamine added to the deposition solution. The black trace gives the absorbance of a stearic acid monolayer on silicon, deposited with LB methods[65].

Water contact angle (CA) (Table 1) revealed that treated samples consistently showed larger CAs than the control NiO_x surface. This is consistent with successful silane attachment and demonstrates that the surface modification of NiO_x directly affected the surface energy. The CA of the OTES treated surface is much higher than that of PTES and 4CPTES treated NiO_x, which was expected, since OTES is very hydrophobic. On the other hand, the CA for OTES on NiO_x is smaller than that of OTES on the native oxide of silicon[68], which is commonly greater than 110°. A high CA is evidence of a densely packed alkyl layer, where the water drop is interacting primarily with the terminal methyl groups[78]. The lower CA value observed here is consistent with a molecular layer that is disordered and/or has incomplete coverage. While the changes in the CA upon adsorption were small (except for OTES), the CAs for all three treatments are in good agreement with what has been previously reported in the literature or measured in our lab for TES surface modification of ZnO (i.e. $72.5° \pm 4.3°$ [65], $97° \pm 13°$ [79], $62° \pm 1°$ [79], for PTES, OTES and 4CPTES, respectively). This suggests that the surface coverage of TES molecules is similar for both NiO_x and ZnO.

Table 1 Contact angles (in degrees) of the control NiO_x and NiO_x treated with three commercially available TES-molecules. The control sample was exposed to the same treatment solution but without TES molecules in the solution

Control	PTES	OTES	4CPTES
42.5 ± 1.4	65.1 ± 0.8	89.5 ± 1.3	63.6 ± 2.9

The contact angle measurements also reinforced our conclusion about the reaction mechanism of TES attachment and its dependence on surface-attached hydroxyl groups. While the CA of as-grown NiO_x was around 50°, this dropped to less than 10° after the 400 C annealing step, which was performed just prior to exposure of the sample to the TES deposition solution.

Kelvin probe contact potential difference (CPD) measurements of control and treated NiO_x were used to determine the change in the work function ($\Delta\phi$) caused by various TES-molecular treatments. This is defined as the work function of treated NiO_x minus the work function of the control NiO_x. As shown in Table 2, NiO_x surfaces treated with all three commercial TES attachments had larger work functions, compared to the control surface. This is an indication that the dipoles resulting from these TES modifiers have their positive ends closer to the surface and their negative ends farther from the surface. With our convention this means that the dipole vector is pointing toward the surface. Also shown in Table 2 are the $\Delta\phi$ values for the same molecular treatments on ZnO, measured on films that were fabricated following the procedure described in Ref. 65. The purpose of this comparison is not to demonstrate quantitative agreement between the work function changes on the two oxides, but to show that the influences of the three surface modifiers follow the same general trends. The integrated FTIR intensity of the C-H modes for OTES on NiO_x, shown in Fig. 4, is approximately 10% smaller than that observed

for OTES on ZnO[65], indicating that the surface coverages for TES attachment on ZnO is similar to, and slightly larger than is observed with NiO_x. For both NiO_x and ZnO the work function of the 4CPTES-treated surface is larger than what results from PTES treatment. This is expected, due to the large electronegativity of chlorine. The relative order of $\Delta\phi$ values on NiO_x for the three molecules is the same as what has been observed on ZnO. However, there are differences. The overall range of the work function change is larger for ZnO, compared to NiO_x. It is also noteworthy that all three molecules increased the NiO_x work function relative to the control while for ZnO, PTES reduced the ZnO work function with OTES and 4CPTES increasing it. In a simple view, the dipole introduced by molecular attachment can be considered to arise from two contributions. The first is the dipole moment of the exposed end group. The second is the dipole introduced by bonding of the TES molecules to the metal oxide surface. This difference between ZnO and NiO_x may arise from a difference in the bonding-related dipole, which would introduce a systematic change in $\Delta\phi$.

Table 2 Change in the work function (in meV) of TES-treated NiO_x, relative to the control NiO_x sample, and of TES-treated ZnO relative to a similar control ZnO sample. A higher $\Delta\phi$ value means the Fermi level of the treated sample is lower in absolute energy, relative to the vacuum energy, due to the TES treatment. The ZnO values were obtained from films produced with methods described in Ref. 65. The experimental uncertainty in these measurements was typically $\sim \pm 30$ meV.

	PTES	OTES	4CPTES
NiO_x	242	302	450
ZnO	-75	225	375

These results with commercially available TES-based molecules demonstrate successful attachment as well as the ability to change the NiO_x work function with different choices of the terminal group. Depending upon the application, larger changes may be important, especially for different active layer materials in BHJ devices where LUMO energy levels can vary by as much as 2.6 eV[80]. For this reason several alternative TES molecules with the potential for larger dipole moments were synthesized. Unlike commercially available PTES, OTES and 4CPTES, the new molecules have an extra conjugated bond connecting the functional group to the TES attachment group. In previous work with phosphonic acid-based molecular modifiers on the ZnO surface, the addition of a double bond at this location was shown to lead to larger dipole moments and work function changes than the unconjugated version of the same molecule. This was attributed to greater delocalization of charge across the entire molecule[81].

Figure 5 shows FTIR absorbance spectra for two of the styryl-based TES molecules in this study, AnTES and CF3TES, attached to NiO_x.

The ring breathing modes are clearly visible at ~ 1100 cm^{-1} indicating the presence of these molecules on the surface. Other significant features include modes at 1037 cm^{-1} (O-CH_3) and 1256 cm^{-1} (aryl-O), in the AnTES spectrum, and modes at 1068 cm^{-1} (aryl-C) and 1328 cm^{-1} (CF_3) in the CF3TES spectrum[82].

The work function change caused by TES molecule attachment to NiO_x was evaluated (by means of the Kelvin probe CPD method) for five newly synthesized molecules. These results were compared to the PTES, OTES and 4CPTES measurements discussed above. The results, shown in Fig. 6 are plotted as a function of the calculated component of the dipole moment along the body axis (partial dipole moment) of the isolated molecules as defined in Fig. 7.

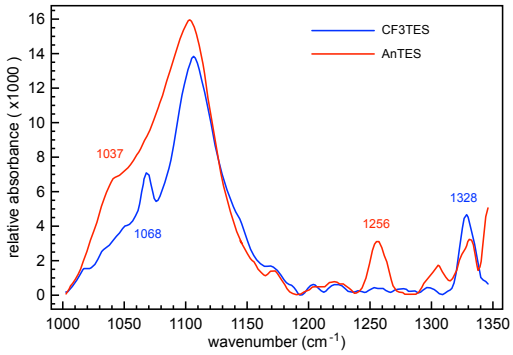

Fig. 5 Infrared absorbance associated with AnTES (red) and CF3TES (blue) on NiO_x.

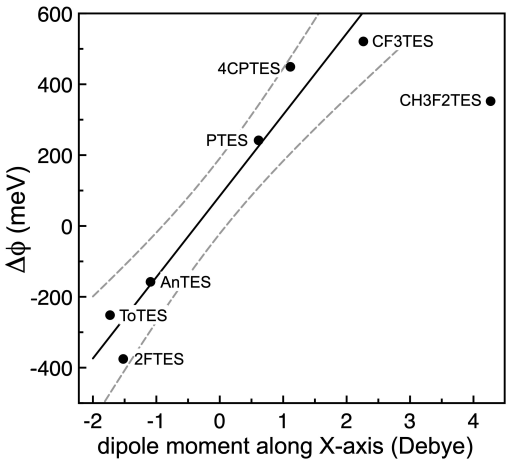

Fig. 6 Work function change of NiO_x after different treatment with triethoxysilanes as a function of partial dipole moment along the body axis of the free molecules. Typical measurement uncertainty in $\Delta\phi$ was $\sim \pm 30$ meV. The line is a linear least-squares fit to all data points except CF3F2TES. The dashed lines identify the 95% confidence interval for the prediction of $\Delta\phi$ versus the dipole moment along the X-axis of the molecule.

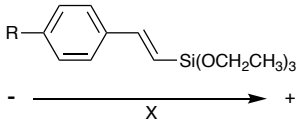

Fig. 7 Chemical structure of the synthesized materials showing the body axis (X-axis) definition and the direction of the calculated dipole moment, defined as positive for the horizontal axis of the graph in Fig. 6.

To demonstrate the reproducibility of the measurements, sam-

ples treated with AnTES and CF3TES were prepared and measured several times to establish an uncertainty range of $\pm$30 meV.

By changing the end group of molecules attached to NiO_x through a TES condensation reaction, the work function of NiO_x can be changed by as much as 900 meV. More importantly, for all the conjugated and non-conjugated TES molecules except CF3F2TES, $\Delta\phi$ correlated well with the calculated magnitude of the partial dipole moment of the isolated molecules. We note that while there was also correlation with the full dipole moment, correlation with the partial moment was much stronger. The calculated moments of many of these molecules had components both along and perpendicular to the X-axis in Fig.7. This suggests the body-axis dipole components primarily contributed to the work function change, which might be expected if the molecules were oriented primarily perpendicular to the surface. The linear fit in Fig. 6 has a slope of 228 meV/D, with an R^2 value of 0.95. This trend is similar to work function changes observed on ZnO and ITO that were treated with conjugated and non-conjugated phosphonic acids.[55] Our molecules accomplish this range of work function changes with stable covalent Ni-O-Si bonds.

The deviation of the work function change for the molecule CF3F2TES from the linear fit in Fig. 6 is interesting. This result was quite reproducible across numerous experimental trials. It could be explained as the result of a less orderly layer with lower coverage or a layer with molecules that were more disordered. However, there is no reason to expect that this molecule would attach with significantly different conditions, compared to the other styryl materials. Since this molecule has the largest dipole moment in the group, a more intriguing speculation is that the molecule more strongly influences the bond with the metal oxide surface. We have previously shown that the conjugated bonds in the styryl group of molecules similar to those used in this study, except with phosphate attachment, allow communication between the terminal species and the surface bond, thereby modifying the surface dipole.[81] The extent of this influence would be strongest with CF3F2TES, leading to a deviation from the systematic relationship demonstrated by the other molecules between the partial dipole moments of the isolated molecules and the respective values of $\Delta\phi$.

The stability of treatments which change the work function of metal oxides for device applications are also of importance. For example, increases in the work function of NiO_x after oxygen plasma treatments have been found to decrease by $\sim$100 meV after just two hours in an inert atmosphere.[25] This was attributed to a possible change in the density of oxygen vacancies or the oxidation state of the Ni in the NiO_x. While an exhaustive long term stability study was beyond the scope of this work, tests were done to check the short term stability of CF3F2TES treatments. Immediately after the CF3F2TES surface treatment, $\Delta\phi$ was measured to be $\sim$350 meV. After resting in an ambient environment for 90 min, $\Delta\phi$ dropped to only 310 meV. Ninety minutes is a sufficiently long working time to allow additional layers to be deposited or additional processing to be completed before the work function changes through exposure to the ambient environment. This indicates that TES surface modification provides a stable method for controlling the work function of NiO_x and, consequently, the energy level alignments between NiO_x and active layer materials in BHJ, perovskite or even heterojunction-with-intrinsic-thin-layer (HIT) solar cells cell devices.

4 Conclusions

We have successfully attached monolayers of covalently bonded TES-molecules with different molecular dipoles to NiO_x, as verified by CA and FTIR measurements. The TES modifiers exhibit sub-monolayer coverage and evidence of disorder. Using TES molecules with a conjugated linkage between the attachment group and the functional end group, we have demonstrated $\sim$ 900 meV changes of the work function of NiO_x. This illustrates the viability of using these molecules to tune the NiO_x work function for better energy level alignment in organic electronic devices. Comparison of DFT calculations of the body axis partial molecular dipole moments and measured work function changes reveal that the two are linearly related. These results underscore the potential of this family of molecules for controlling NiO_x properties in applications where interfacial energetics are critical, and also suggest the benefit of computational prediction in the design of such surfaces for device applications.

5 Acknowledgement

The authors acknowledge valuable discussion with Erin Ratcliff and assistance from Bo Wang and Erich Meinig. We also thank the National Renewable Energy Laboratory (NREL) for access to the Kelvin probe instrument and the organic photovoltaic lab. G. C. thanks Jennifer Braid for Kelvin probe assistance, and Darick Baker for training on the TES treatment protocol. This research is based upon work supported in part by the National Science Foundation under grant No. 0907409 and the Solar Energy Research Institute for India and the U.S. (SERIIUS) funded jointly by the U.S. Department of Energy subcontract DE AC36-08G028308 (Office of Science, Office of Basic Energy Sciences, and Energy Efficiency and Renewable Energy, Solar Energy Technology Program, with support from the Office of International Affairs) and the Government of India subcontract IUSSTF/JCERDC-SERIIUS/2012 dated 22nd Nov. 2012. D.C.O.'s research was funded by the U.S. Department of Energy under Contract DE-AC36-08-GO28308 with the National Renewable Energy Laboratory through the DOE SETO program.

References

1 A. J. Heeger, *Advanced Materials*, 2014, **26**, 10–28.
2 N. Marinova, S. Valero and J. L. Delgado, *Journal of Colloid and Interface Science*, 2017, **488**, 373–389.
3 B. Fan, X. Du, F. Liu, W. Zhong, L. Ying, R. Xie, X. Tang, K. An, J. Xin, N. Li, W. Ma, C. J. Brabec, F. Huang and Y. Cao, *Nature Energy*, 2018, **3**, 1051–1058.
4 H. Kang, G. Kim, J. Kim, S. Kwon, H. Kim and K. Lee, *Advanced Materials*, 2016, **28**, 7821–7861.
5 A. Wadsworth, M. Moser, A. Marks, M. S. Little, N. Gasparini, C. J. Brabec, D. Baran and I. McCulloch, *Chemical Society Reviews*, 2019, **48**, 1596–1625.
6 J. Yuan, Y. Zhang, L. Zhou, G. Zhang, H.-L. Yip, T.-K. Lau,

X. Lu, C. Zhu, H. Peng, P. A. Johnson, M. Leclerc, Y. Cao, J. Ulanski, Y. Li and Y. Zou, *Joule*, 2019, **3**, 1140–1151.

7 E. L. Ratcliff, B. Zacher and N. R. Armstrong, *Journal of Physical Chemistry Letters*, 2011, **2**, 1337–1350.

8 W. Deng, X. Liang, P. S. Kubiak and P. J. Cameron, *Advanced Energy Materials*, 2018, **8**, 1701544.

9 Z. Yin, J. Wei and Q. Zheng, *Advanced Science*, 2016, **3**, 1500362.

10 K. Kawano, R. Pacios, D. Poplavskyy, J. Nelson, D. D. C. Bradley and J. R. Durrant, *Solar Energy Materials and Solar Cells*, 2006, **90**, 3520–3530.

11 K. Norrman, M. V. Madsen, S. A. Gevorgyan and F. C. Krebs, *Journal of the American Chemical Society*, 2010, **132**, 16883–16892.

12 Y.-H. Kim, S.-H. Lee, J. Noh and S.-H. Han, *Thin Solid Films*, 2006, **510**, 305–310.

13 M. P. de Jong, L. J. van IJzendoorn and M. J. A. de Voigt, *Applied Physics Letters*, 2000, **77**, 2255–2257.

14 J. Meyer, S. Hamwi, M. Kröger, W. Kowalsky, T. Riedl and A. Kahn, *Advanced Materials*, 2012, **24**, 5408–5427.

15 A. K. Kyaw, X. W. Sun, C. Y. Jiang, G. Q. Lo, D. W. Zhao and D. L. Kwong, *Applied Physics Letters*, 2008, **93**, 40–42.

16 C. Girotto, E. Voroshazi, D. Cheyns, P. Heremans and B. P. Rand, *ACS Applied Materials and Interfaces*, 2011, **3**, 3244–3247.

17 J. Meyer, K. Zilberberg, T. Riedl and A. Kahn, *Journal of Applied Physics*, 2011, **110**, 33710.

18 K. Zilberberg, S. Trost, J. Meyer, A. Kahn, A. Behrendt, D. Lützenkirchen-Hecht, R. Frahm and T. Riedl, *Advanced Functional Materials*, 2011, **21**, 4776–4783.

19 K. Zilberberg, S. Trost, H. Schmidt and T. Riedl, *Advanced Energy Materials*, 2011, **1**, 377–381.

20 T. Stubhan, N. Li, N. A. Luechinger, S. C. Halim, G. J. Matt and C. J. Brabec, *Advanced Energy Materials*, 2012, **2**, 1433–1438.

21 Z. Tan, L. Li, C. Cui, Y. Ding, Q. Xu, S. Li, D. Qian and Y. Li, *The Journal of Physical Chemistry C*, 2012, **116**, 18626–18632.

22 H. Choi, B. Kim, M. J. Ko, D.-K. Lee, H. Kim, S. H. Kim and K. Kim, *Organic Electronics*, 2012, **13**, 959–968.

23 M. Y. Chan, C. S. Lee, S. L. Lai, M. K. Fung, F. L. Wong, H. Y. Sun, K. M. Lau and S. T. Lee, *Journal of Applied Physics*, 2006, **100**, 94506.

24 K. X. Steirer, J. P. Chesin, N. E. Widjonarko, J. J. Berry, A. Miedaner, D. S. Ginley and D. C. Olson, *Organic Electronics*, 2010, **11**, 1414–1418.

25 K. X. Steirer, P. F. Ndione, N. E. Widjonarko, M. T. Lloyd, J. Meyer, E. L. Ratcliff, A. Kahn, N. R. Armstrong, C. J. Curtis, D. S. Ginley, J. J. Berry and D. C. Olson, *Advanced Energy Materials*, 2011, **1**, 813–820.

26 K. X. Steirer, R. E. Richards, A. K. Sigdel, A. Garcia, P. F. Ndione, S. Hammond, D. Baker, E. L. Ratcliff, C. Curtis, T. Furtak, D. S. Ginley, D. C. Olson, N. R. Armstrong and J. J. Berry, *Journal of Materials Chemistry A*, 2015, **3**, 10949–10958.

27 E. L. Ratcliff, J. Meyer, K. X. Steirer, N. R. Armstrong, D. Olson and A. Kahn, *Organic Electronics*, 2012, **13**, 744–749.

28 J.-Y. Jeng, K.-C. Chen, T.-Y. Chiang, P.-Y. Lin, T.-D. Tsai, Y.-C. Chang, T.-F. Guo, P. Chen, T.-C. Wen and Y.-J. Hsu, *Advanced Materials*, 2014, **26**, 4107–4113.

29 J. R. Manders, S.-W. Tsang, M. J. Hartel, T.-H. Lai, S. Chen, C. M. Amb, J. R. Reynolds and F. So, *Advanced Functional Materials*, 2013, **23**, 2993–3001.

30 J. You, L. Meng, T.-B. Song, T.-F. Guo, Y. M. Yang, W.-H. Chang, Z. Hong, H. Chen, H. Zhou, Q. Chen, Y. Liu, N. De Marco and Y. Yang, *Nature Nanotechnology*, 2016, **11**, 75–81.

31 M. B. Islam, M. Yanagida, Y. Shirai, Y. Nabetani and K. Miyano, *ACS Omega*, 2017, **2**, 2291–2299.

32 R. Islam, G. Shine and K. C. Saraswat, *Applied Physics Letters*, 2014, **105**, 182103.

33 J. J. Berry, N. E. Widjonarko, B. A. Bailey, A. K. Sigdel, D. S. Ginley and D. C. Olson, *IEEE Journal on Selected Topics in Quantum Electronics*, 2010, **16**, 1649–1655.

34 R. Islam, G. Chen, P. Ramesh, J. Suh, N. Fuchigami, D. Lee, K. A. Littau, K. Weiner, R. T. Collins and K. C. Saraswat, *ACS Applied Materials and Interfaces*, 2017, **9**, 17201–17207.

35 M. T. Greiner, M. G. Helander, Z. B. Wang, W. M. Tang and Z. H. Lu, *Journal of Physical Chemistry C*, 2010, **114**, 19777–19781.

36 S. Liu, R. Liu, Y. Chen, S. Ho, J. H. Kim and F. So, *Chemistry of Materials*, 2014, **26**, 4528–4534.

37 A. Liu, G. Liu, H. Zhu, B. Shin, E. Fortunato, R. Martins and F. Shan, *Applied Physics Letters*, 2016, **108**, 233506.

38 C. Hu, K. Chu, Y. Zhao and W. Y. Teoh, *ACS Applied Materials and Interfaces*, 2014, **6**, 18558–18568.

39 R. Kumar, C. Baratto, G. Faglia, G. Sberveglieri, E. Bontempi and L. Borgese, *Thin Solid Films*, 2015, **583**, 233–238.

40 H.-L. Yip, S. K. Hau, N. S. Baek, H. Ma and A. K.-Y. Jen, *Advanced Materials*, 2008, **20**, 2376–2382.

41 S. Blumstengel, H. Glowatzki, S. Sadofev, N. Koch, S. Kowarik, J. P. Rabe and F. Henneberger, *Physical Chemistry Chemical Physics*, 2010, **12**, 11642–11646.

42 Y. E. Ha, M. Y. Jo, J. Park, Y. C. Kang, S. I. Yoo and J. H. Kim, *Journal of Physical Chemistry C*, 2013, **117**, 2646–2652.

43 T. M. Brenner, G. Chen, E. P. Meinig, D. J. Baker, D. C. Olson, R. T. Collins and T. E. Furtak, *Journal of Materials Chemistry C*, 2013, **1**, 5935–5943.

44 I. Lange, S. Reiter, M. Pätzel, A. Zykov, A. Nefedov, J. Hildebrandt, S. Hecht, S. Kowarik, C. Wöll, G. Heimel and D. Neher, *Advanced Functional Materials*, 2014, **24**, 7014–7024.

45 S. R. Cowan, P. Schulz, A. J. Giordano, A. Garcia, B. A. Macleod, S. R. Marder, A. Kahn, D. S. Ginley, E. L. Ratcliff and D. C. Olson, *Advanced Functional Materials*, 2014, **24**, 4671–4680.

46 I. Lange, S. Reiter, J. Kniepert, F. Piersimoni, M. Pätzel, J. Hildebrandt, T. Brenner, S. Hecht and D. Neher, *Applied Physics Letters*, 2015, **106**, 1–5.

47 R.-X. Ou, Y.-C. Chen, C.-H. Lin, T.-F. Guo and T.-C. Wen, *Organic Electronics*, 2018, **63**, 93–97.

48 C. Ganzorig, K. J. Kwak, K. Yagi and M. Fujihira, *Applied Physics Letters*, 2001, **79**, 272–274.

49 E. L. Bruner, N. Koch, A. R. Span, S. L. Bernasek, A. Kahn and J. Schwartz, *Journal of the American Chemical Society*, 2002, **124**, 3192–3193.

50 S. Khodabakhsh, D. Poplavskyy, S. Heutz, J. Nelson, D. D. Bradley, H. Murata and T. S. Jones, *Advanced Functional Materials*, 2004, **14**, 1205–1210.

51 J. S. Kim, J. H. Park, J. H. Lee, J. Jo, D. Y. Kim and K. Cho, *Applied Physics Letters*, 2007, **91**, 4–6.

52 N. R. Armstrong, P. A. Veneman, E. Ratcliff, D. Placencia, M. Brumbach and C. O. N. Spectus, *Accounts of Chemical Research*, 2009, **42**, 1748–1757.

53 A. Sharma, P. J. Hotchkiss, S. R. Marder and B. Kippelen, *Journal of Applied Physics*, 2009, **105**, 1–6.

54 P. J. Hotchkiss, S. C. Jones, S. A. Paniagua, A. Sharma, B. Kippelen, N. R. Armstrong and S. R. Marder, *Accounts of Chemical Research*, 2012, **45**, 337–346.

55 U. Koldemir, J. L. Braid, A. Morgenstern, M. Eberhart, R. T. Collins, D. C. Olson and A. Sellinger, *The Journal of Physical Chemistry Letters*, 2015, **6**, 2269–2276.

56 S. A. Paniagua, A. J. Giordano, O. L. Smith, S. Barlow, H. Li, N. R. Armstrong, J. E. Pemberton, J.-L. Brédas, D. Ginger and S. R. Marder, *Chemical Reviews*, 2016, **116**, 7117–7158.

57 M. Timpel, H. Li, M. V. Nardi, B. Wegner, J. Frisch, P. J. Hotchkiss, S. R. Marder, S. Barlow, J.-L. Brédas and N. Koch, *Advanced Functional Materials*, 2018, **28**, 1704438.

58 A. Gankin, E. Mervinetsky, I. Alshanski, J. Buchwald, A. Dianat, R. Gutierrez, G. Cuniberti, R. Sfez and S. Yitzchaik, *Langmuir*, 2019, **35**, 2997–3004.

59 Q. Wang, C. C. Chueh, T. Zhao, J. Cheng, M. Eslamian, W. C. Choy and A. K. Jen, *ChemSusChem*, 2017, **10**, 3794–3803.

60 Y. Cheng, M. Li, X. Liu, S. H. Cheung, H. T. Chandran, H.-W. Li, X. Xu, Y.-M. Xie, S. K. So, H.-L. Yip and S.-W. Tsang, *Nano Energy*, 2019, **61**, 496–504.

61 A. Bulusu, S. A. Paniagua, B. A. MacLeod, A. K. Sigdel, J. J. Berry, D. C. Olson, S. R. Marder and S. Graham, *Langmuir*, 2013, **29**, 3935–3942.

62 S. Hietzschold, S. Hillebrandt, F. Ullrich, J. Bombsch, V. Rohnacher, S. Ma, W. Liu, A. Köhn, W. Jaegermann, A. Pucci, W. Kowalsky, E. Mankel, S. Beck and R. Lovrincic, *ACS Applied Materials and Interfaces*, 2017, **9**, 39821–39829.

63 J. Mangalam, T. Rath, S. Weber, B. Kunert, T. Dimopoulos, A. Fian and G. Trimmel, *Journal of Materials Science: Materials in Electronics*, 2019, **30**, 9602–9611.

64 O. Taratula, E. Galoppini, D. Wang, D. Chu, Z. Zhang, H. Chen, G. Saraf and Y. Lu, *The Journal of Physical Chemistry B*, 2006, **110**, 6506–6515.

65 C. G. Allen, D. J. Baker, J. M. Albin, H. E. Oertli, D. T. Gillaspie, D. C. Olson, T. E. Furtak and R. T. Collins, *Langmuir*, 2008, **24**, 13393–13398.

66 P. Schulz, S. R. Cowan, Z.-L. Guan, A. Garcia, D. C. Olson and A. Kahn, *Advanced Functional Materials*, 2013, **24**, 701–706.

67 A. Garcia, G. C. Welch, E. L. Ratcliff, D. S. Ginley, G. C. Bazan and D. C. Olson, *Advanced Materials*, 2012, **24**, 5368–5373.

68 D. Walba, C. Liberko, E. Korblova, M. Farrow, T. Furtak, B. Chow, D. Schwartz, A. Freeman, K. Douglas, S. Williams, A. Klittnick and N. Clark, *Liquid Crystals*, 2004, **31**, 481–489.

69 M. Egashira, S. Kawasumi, S. Kagawa and T. Seiyama, *Bulletin of the Chemical Society of Japan*, 1978, **51**, 3144–3149.

70 M. Egashira, M. Nakashima, S. Kawasumi and T. Selyama, *The Journal of Physical Chemistry*, 1981, **85**, 4125–4130.

71 J. C. de Jesús, J. Carrazza, P. Pereira and F. Zaera, *Surface Science*, 1998, **397**, 34–47.

72 S. Oyola-Reynoso, I. D. Tevis, J. Chen, B. S. Chang, S. Çinar, J.-F. Bloch and M. M. Thuo, *Journal of Materials Chemistry A*, 2016, **4**, 14729–14738.

73 A. F. Stalder, G. Kulik, D. Sage, L. Barbieri and P. Hoffmann, *Colloids and Surfaces A*, 2006, **286**, 92–103.

74 F. S. Benneckendorf, S. Hillebrandt, F. Ullrich, V. Rohnacher, S. Hietzschold, D. Jänsch, J. Freudenberg, S. Beck, E. Mankel, W. Jaegermann, A. Pucci, U. H. F. Bunz and K. Müllen, *The Journal of Physical Chemistry Letters*, 2018, **9**, 3731–3737.

75 R. A. MacPhail, H. L. Strauss, R. G. Snyder and C. A. Eiliger, *Journal of Physical Chemistry*, 1984, **88**, 334–341.

76 A. N. Parikh, D. L. Allara, I. B. Azouz and F. Rondelez, *Journal of Physical Chemistry*, 1994, **98**, 7577–7590.

77 R. G. Snyder, H. L. Strauss and C. A. Elliger, *Journal of Physical Chemistry*, 1982, **86**, 5145–5150.

78 A. Ulman, *Chemical Reviews*, 1996, **96**, 1533–1554.

79 C. G. Allen, D. J. Baker, T. M. Brenner, C. C. Weigand, J. M. Albin, K. X. Steirer, D. C. Olson, C. Ladam, D. S. Ginley, R. T. Collins and T. E. Furtak, *The Journal of Physical Chemistry C*, 2012, **116**, 8872–8880.

80 X. Fan, M. Zhang, X. Wang, F. Yang and X. Meng, *Journal of Materials Chemistry A*, 2013, **1**, 8694.

81 J. L. Braid, U. Koldemir, A. Sellinger, R. T. Collins, T. E. Furtak and D. C. Olson, *ACS Applied Materials and Interfaces*, 2014, **6**, 19229–34.

82 D. Lin-Vien, N. Colthup, W. Fateley and J. Grasselli, *The Handbook of Infrared and Raman Characteristic Frequencies of Organic Molecules*, Academic Press, San Diego, CA, 1991, pp. 1–503.

We have synthesized a family of styryl-based molecules that have been attached to nickel oxide films using a novel ethoxysilane chemistry to modify the work function over a range of 900 meV.

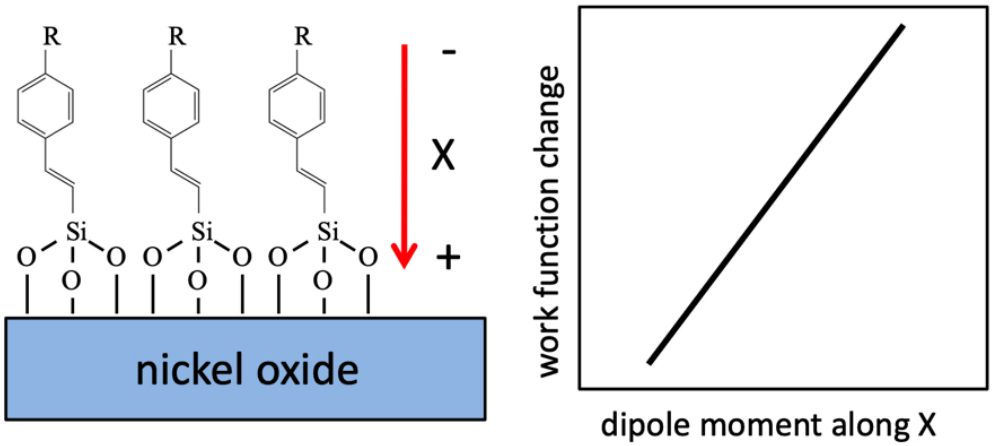

75x34mm (300 x 300 DPI)